Hubble Space Telescope observations of an extraordinary flare in the M87 jet[1]

Juan P. Madrid [2,3]

ABSTRACT

HST-1, a knot along the M87 jet located $0.85''$ from the nucleus of the galaxy has experienced dramatic and unexpected flaring activity since early 2000. We present analysis of Hubble Space Telescope Near-Ultraviolet (NUV) imaging of the M87 jet from 1999 May to 2006 December that reveals that the NUV intensity of HST-1 has increased 90 times over its quiescent level and outshines the core of the galaxy. The NUV light curve that we derive is synchronous with the light curves derived in other wavebands. The correlation of X-ray and NUV light curves during the HST-1 flare confirms the synchrotron origin of the X-ray emission in the M87 jet. The outburst observed in HST-1 is at odds with the common definition of AGN variability usually linked to blazars and originating in close proximity of the central black hole. In fact, the M87 jet is not aligned with our line of sight and HST-1 is located at one million Schwarzchild radii from the super-massive black hole in the core of the galaxy.

Subject headings: galaxies: jets - galaxies: active

1. Introduction

M87, the cD galaxy of the Virgo cluster, is a giant elliptical famed for its spectacular galactic-scale plasma jet. Due to its proximity, images of M87's jet at high resolution have revealed a profusion of distinct knots or regions of enhanced emission along the whole length of the jet. These knots have been clearly detected at radio, optical, UV, and X-ray wavelengths. The detection of these UV and X-ray emission regions hundreds of parsecs away

---

[2]Space Telescope Science Institute, 3700 San Martin Drive, Baltimore, MD 21218

[3] Now at Department of Physics and Astronomy, McMaster University, Hamilton, ON, L8S 4M1, Canada

from the AGN proves that these are regions of in situ particle acceleration within the jet because such high energy emission vanishes rapidly. The radiative half-lives of synchrotron X-ray emitting electrons are of the order of years, and the cooling time for UV emitting particles are of the order of decades (Harris & Krawczynski 2006). High energy emission would be confined in a small space without re-acceleration along the jet. Thus these knots must be regions of acceleration distinct from the AGN.

Until February 2000 HST-1 was an inconspicuous knot of the M87 jet located $0.85''$ from the nucleus of the galaxy (Waters & Zepf 2005). Since that date, HST-1 has shown an unexpectedly rapid variability in all wavebands. More strikingly, in 2003 HST-1 became brighter than the nucleus of the galaxy, which is known to harbor a super-massive black hole of $3.2 \pm 0.9 \times 10^9 M_\odot$(Macchetto et al. 1997). HST-1 is also the most probable site of production of the TeV γ rays emanating from M87 recently reported by the HESS collaboration (Aharonian et al. 2006, see also Cheung et al. 2007).

Specific observations of HST-1 have been carried out across the electromagnetic spectrum, and a particularly detailed study of the flaring of HST-1 has been conducted with the Chandra X-ray Observatory by D. E. Harris and collaborators (Harris et al. 2003, 2006, 2008). The X-ray intensity of this peculiar knot has increased more than 50 times in the past five years and peaked in 2005. There is a wealth of high-quality HST NUV imaging data of the M87 jet that has been only succinctly presented in the past (Madrid et al. 2007). The NUV light-curve for HST-1 that we present here has broadly the same shape as the X-ray light curve presented by Harris et al. (2006): the flare rises, peaks, and declines simultaneously in the X-rays and the NUV.

HST-1 is located at one million Schwarzchild radii away from the galactic nucleus but if M87 were at a greater distance, or if our telescopes had lesser resolution, this flare would have been interpreted as variability intrinsic to the central black hole and its immediate vicinity. This blazar-like behavior is clearly isolated from the central engine and it is not directly beamed as the M87 jet is misaligned with respect to the line of sight (Harris et al. 2006, Cheung et al. 2007). A detailed characterization of this flare is thus important to better understand blazar variability.

We describe the Hubble Space Telescope view of the remarkable flaring of the HST-1 knot with high resolution imaging taken over more than seven years of observations and aim to present the visually striking NUV data that bridges the gap between the X-ray (Harris et al. 2006) and radio (Cheung et al. 2007) observations of HST-1.

2.   Observations & Data Reduction

We present observations obtained with two instruments on board HST: the Space Telescope Imaging Spectrograph (STIS) and the Advanced Camera for Surveys (ACS).

STIS stopped functioning in 2004 August due to an electronics failure on the redundant (Side 2) power supply system. All observations after August 2004 were taken with the ACS. Even though each of these two instruments has unique characteristics, they cover the same wavebands and provide data that are easily compared. Moreover, the ACS images have the same file structure as STIS images making the data reduction procedure very similar between the two instruments. The discrepancy between the STIS and the ACS absolute photometric calibration does not exceed 2% (Bohlin, 2007).

The STIS observations were carried out using the NUV/MAMA detector which has a field of view of $24.7'' \times 24.7''$ and a $0.024''$ pixel size. The M87 jet was imaged with the F25QTZ filter that has its maximum throughput wavelength at 2364.8Å and a width of 995.1Å. Due to the nature of the detector NUV/MAMA images are free of cosmic rays (Kim Quijano, 2003).

The ACS High Resolution Camera (HRC) is a CCD instrument with a field of view of $29'' \times 25''$ and a scale of $\sim 0.025''$ per pixel. We analyze images acquired with the F220W and F250W filters, which are the two broadband NUV filters with the most similar characteristics to the STIS F25QTZ filter. The F220W filter has its pivot wavelength at 2255.5Å and a width of 187.3Å, for the F250W these values are 2715.9Å and 239.4Å respectively (Mack et al. 2003, Gonzaga et al. 2005).

We obtained the flatfielded science files (FLT) from the HST public archive for data acquired by both instruments. These science ready files are processed through the automatic reduction and calibration pipeline (CALACS) before they are retrieved from the public archive. The pipeline subtracts the bias and dark current and applies the flatfield to the raw CCD data (Sirianni et al. 2005). Subsequent data reduction was performed using the software package Space Telescope Science Data Analysis System (STSDAS).

We analyzed data taken over a period of time of more than seven years, from 1999 May, through 2006 December. Each image, at all epochs, is the product of the combination of four single exposures taken within the same orbit. This allows us to eliminate cosmic rays in the ACS images and improve the signal to noise.

We used the STSDAS task MULTIDRIZZLE to apply the geometric distortion correction, eliminate cosmic rays, and align and combine the individual exposures of every epoch. The distortion correction was computed with up-to-date distortion coefficient tables retrieved

from the Multimission Archive at the Space Telescope (MAST). During the data reduction process we preserved the native pixel size. The final output images generated by MULTIDRIZ-ZLE have units of counts per second for the STIS data, and units of electrons per second for the ACS data (Koekemoer et al. 2002).

We derive fluxes and errors by doing aperture photometry with PHOT with and aperture radius of 10 pixels or $0.25''$. At the distance of M87, 16.1 Mpc (Tonry et al. 2001), $1''$ corresponds to 77pc. We convert the number of counts obtained with PHOT into flux and flux errors by using PHOTFLAM, or inverse sensitivity, for each instrument found in the updated ACS zeropoint tables maintained by the STScI, or in the header of the STIS images:

$$\mathrm{PHOTFLAM}_{STIS/F25QTZ} = 5.8455.10^{-18} \text{ erg cm}^{-2} \text{ Å}$$

$$\mathrm{PHOTFLAM}_{ACS/F220W} = 8.0721.10^{-18} \text{ erg cm}^{-2} \text{ Å}$$

$$\mathrm{PHOTFLAM}_{ACS/F250W} = 4.7564.10^{-18} \text{ erg cm}^{-2} \text{ Å}$$

Once the calibrated fluxes and poisson errors are derived they are transformed into miliJanskys using the pyraf task CALCPHOT of the synthetic photometry (SYNPHOT) software package under STSDAS. We also scale the flux measurements obtained with different bands using SYNPHOT (Laidler et al. 2005). We expect that no additional errors are introduced by SYNPHOT when doing the transformation to miliJanskys. We assume that the spectrum of HST-1 is described by a power law with index α (Perlman et al. 2001), and we define the flux density as $S_\nu \propto \nu^{-\alpha}$.

The background light was estimated by measuring the flux with the same circular aperture at the same radial distance from the nucleus than HST-1, but on the side of the jet. The aperture corrections were performed using the values published by Proffitt et al. (2003) for STIS and Sirianni et al. (2005) for the ACS. We use the reddening towards M87 determined by Schlegel et al. (1998), E(B-V)=0.022, and the extinction relations from Cardelli et al. (1989) to derive the extinction in the HST filters. We find the following values for the extinction: $A_{F25QTZ} = 0.190$, $A_{F220W} = 0.220$, and $A_{F250W} = 0.134$.

3. Results

HST-1 was dormant until 2000 February when its flaring activity began (Waters & Zepf 2003). We see this in Figure 1 which is a zoom of the inner regions of the M87 jet and

displays, on the left, the early evolution of HST-1. Three main emission loci are visible in this zoom, from left to right, these are: the nucleus of the galaxy, HST-1, and knot D. The images in the left column of Fig. 1 were acquired with STIS/F25QTZ while the images on the right column were taken with the ACS in the F220W band.

In the STIS image of 1999 May (top left) HST-1 was an unremarkable knot along the M87 jet. The brightening of HST-1 is already noticeable in 2001 July. The images in the lower left were taken in 2002 February and 2002 July respectively and show the slow brightening of HST-1 during this year. At the end of 2002 HST-1 is 15 times brighter than in 1999 May.

In 2003 HST-1 became dramatically variable. The image on the top right was taken on 2003 April as HST-1 continues to rise in flux. HST-1 is at its highest recorded brightness in 2005 May, on this date we recorded the highest flux of HST-1 in the NUV, namely 0.54 mJy. At this point in time the NUV flux of HST-1 was four times the measured flux of the central engine of the galaxy. The peak of the X-ray flux based on Chandra observations was reported on 2005 April (Harris et al. 2006). HST-1 attained a NUV flux 90 times its quiescent level in 2005 May. The HST data acquired in 1999 gives us a measure of the brightness of HST-1 during its latent state and allow us to measure the total factor by which the brightness changed during the outburst. Chandra was just launched in 1999 and VLBI radio observations date back to 2000 only (Cheung et al. 2007).

After May 2005 HST-1 declined in intensity with a decay time similar to the rise time. HST-1 experienced a second and also unexpected outburst in 2006 November. This second outburst is fainter than the first one in 2005 May. The image on the lower right of Fig. 1 shows HST-1 during the second, yet fainter, outburst in 2006 November. It is evident from Figure 1 that the jet itself is better mapped by the STIS images.

Table 1 present the log of observations of the M87 jet taken with STIS and ACS. This table also presents the NUV intensities and poisson errors of the nucleus of the galaxy and HST-1 at all epochs studied here. Although magnitudes of the Space Telescope system or erg/s/cm^2/Hz would be more natural units we decided to plot our light curve in mJy to facilitate comparison with observations at other wavebands (Waters & Zepf 2005, Perlman et al. 2003, Harris et al. 2006).

Figure 2 shows the light curve of HST-1 and the nucleus of the galaxy. The HST-1 light curve is bumpy in the radio and the X-rays and the NUV is not an exception. The dramatic flaring of HST-1 can be clearly appreciated in this figure.

Table 2 contains the doubling and halving times for HST-1 calculated for the NUV following the prescriptions of Harris et al (2006). We calculate $y = I_2/I_1$, the flux ratio, and

the time elapsed, Δt, between two consecutive observations. The doubling time is calculated using DT=$[\frac{1}{y-1}]\Delta t$ and the halving time by HT=$[\frac{0.5}{1-y}]\Delta t$. The bumpiness attributed to synchrotron losses in the X-ray persists in the NUV. These rapid variations of brightness are consistent with the month time-scale variability reported by Perlman et al. (2003) for the early stages of the flare and found here to persist through time.

The X-ray and NUV light curves of HST-1 are plotted together in Figure 3. We performed a formal correlation analysis of these two light curves by taking thirty simultaneous values of the NUV and X-ray fluxes and deriving the Spearman rank correlation coefficient ρ. This coefficient is a non parametric measure of correlation and the range is $0 < \rho < 1$, the higher the value, the more significant the correlation (Wall & Jenkins 2003). Simultaneous measurements of the flux of HST-1 in the X-ray and the NUV yield $\rho = 0.966$ reflecting a strong correlation.

4. Discussion

In Harris et al. (2003) synchrotron loss models based on the NUV data available at that time predicted the optical decay time of the flare to be a factor of 10 larger than the X-ray decay time. On the other hand, Perlman et al. (2003) forethought a similar decay timescale for both optical and X-ray lighcurves.

The simultaneous rise and fall of the flare at NUV and X-ray wavelengths supports the first plausible hypothesis of the physical origin of the HST-1 flare postulated by Harris et al. (2006), namely, that a simple compression caused the HST-1 outburst. Compression increases both the magnetic field strength and particle energy at all wavelengths equally, leading to simultaneous flaring at all wavebands. The magnetic field vectors in HST-1 are perpendicular to the jet direction also consistent with a shock (Perlman et al. 2003).

The overall rise and fall timescales, similar in both bands, and the lack of a large delay between bands suggest a rapid expansion as a probable cause for the decrease in luminosity. However, a more rigorous analysis of the rise and fall timescales shows that expansion is not the dominant mechanism of energy loss for HST-1, see below (Harris et al. 2008).

A more elaborated theoretical interpretation for the origin of HST-1 was presented by Stawarz et al. (2006) and supported by the observations of Cheung et al.(2007). This newer hypothesis claims that HST-1 originates in a nozzle throat of the M87 jet that creates reconfinement of magnetic field lines liberating large amounts of energy, similar to the process responsible for solar flares. The gravitational influence of the central AGN on the velocity dispersion of the stars in the innermost regions of this galaxy has been well documented with

early HST observations (Lauer et al. 1992, see also Macchetto et al. 1997). The hot thermal gas can be expected to follow the distribution of the stars in this inner region and create a reconfinement shock in the jet due to an enhanced thermal pressure. This reconfinement should happen at roughly the same distance of the well known stellar cusp, precisely where HST-1 lays (Stawarz et al. 2006).

The doubling and halving time scales of the NUV presented in this paper and the X-rays ones published by Harris et al. (2006) do not always perfectly overlap in time, the HST and Chandra observations were not taken simultaneously. However, it is evident from the values of Table 2 and the values of Tables 3 and 6 of Harris et al. (2006) that the rise and fall timescales are consistently larger in the NUV than in the X-rays. See, for instance, the time interval between 2005 June 21 and 2005 August 06 when halving time for the X-rays is 0.21 while in the NUV between 2005 June 22 and 2005 August 01 the decay time is 0.36. Harris et al. (2008) make a detailed analysis of rise and fall time scales for HST-1 and conclude that this longer decay time in the NUV is an indication that expansion is not the primary energy loss mechanism for the charged particles emitting within the HST-1 region.

The detection of polarized emission as well as synchrotron emission models fitted to flux measurements provided evidence that the physical process responsible for the radio to UV emission in the knots of the M87 jet is synchrotron radiation of electrons accelerated by the magnetic field of the jet (Perlman et al. 2001). The very strong correlation between the NUV and X-ray light curves of the HST-1 flare proves that the same physical phenomenon and the same electrons are responsible for the emission in both bands. Therefore the X-ray emission is also synchrotron in origin. The injection of fresh particles into the flaring volume is not needed to explain the high-energy emission, the X-ray emission is well interpreted as the high energy extension of the radio to optical spectrum (Perlman & Wilson 2005, Harris et al. 2006). The observations presented here rules out inverse Compton (IC) up-scattering of lower energy electrons, as the cause of the high energy emission of this flare in particular, and of the other emission knots along the M87 jet. Moreover, high-energy photons produced by IC up-scattering would take much longer (10000 years) than the observed time to decrease in flux (Harris, 2003).We can thus safely state that synchrotron emission is the physical process responsible for the high energy emission in the M87 jet.

The encircled energy distribution of HST-1 follows the pattern of the detectors PSF at all epochs. In the NUV, HST-1 remains unresolved with an upper limit on its size of $\sim 0.025''$, i. e. $\sim 1.9 pc$.

The HESS collaboration recently reported a detection of TeV γ rays emanating from M87, but the Cherenkov telescopes used for this detection lack the resolution to determine the exact position of the TeV emitting region. Cheung et al. (2007) favor HST-1 over

the nucleus as the site of origin of the TeV emission. They note that the light curve of TeV emission in M87 is roughly similar to the light curve of the HST-1 flare seen in the radio and X-ray. The NUV peaks simultaneously with the X-rays and the γ rays and only HST-1 shows a flaring behavior in the NUV. The nucleus shows only the characteristic low amplitude variability, see Figure 2. These facts support the hypothesis of HST-1 as the site of origin of the γ rays through IC upscattering of ambient photons by high-energy electrons produced during the outburst.

After 2003 May, and for more than four years, the flux of HST-1 dominates the NUV emission of M87, patently overpowering the emission of the central engine (see Fig. 3). Given that within radio galaxies the principal sources of particle acceleration are the core and the jet, the large flux from this flare plays, as we have shown here, a crucial role determining the NUV flux and therefore the spectrum of the entire galaxy.

As part of the Chandra Cen A Very Large Project Hardcastle et al. (2007) searched, to no avail, for HST-1-like variability in the X-ray jet of this galaxy (D=3.7Mpc). Hardcastle et al. aimed at answering an important question: Is HST-1 a feature unique of M87? Or is this extreme variability ubiquitous, or at least frequent, in AGN jets? If an HST-1-type outburst occurred in more distant AGN, it would not be resolved with current optical and X-ray instruments and would probably be associated with Doppler boosting of emission emanating from a jet close to the line of sight or with events associated to variability of the accretion disk of the black hole. However, the angle of the M87 jet with the line of sight is about 26-30 deg (Cheung et al. 2007, Bicknell & Begelman 1996) allowing only a modest beaming. Also, given its large distance from the core, i.e. more than 65 pc or one million Schwarzchild radii, intrinsic black hole variability has no direct relation with this flaring. Outbursts similar to HST-1 can be responsible for variability associated with high redshift blazars but remain completely unresolved.
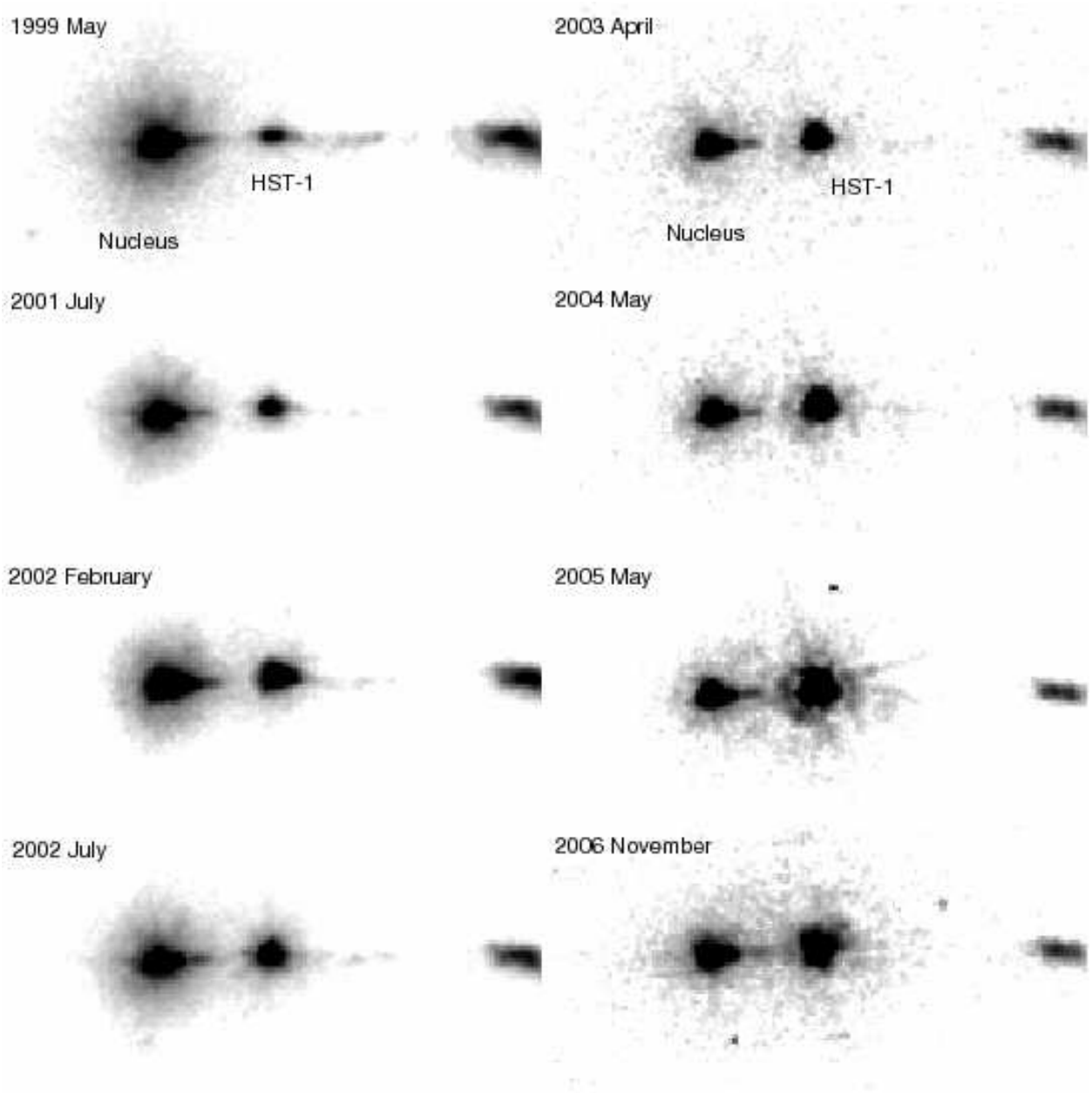
Fig. 1.— Observations of the inner jet of M87 taken with the STIS/F25QTZ (left column) and the ACS/F220W (right column). The nucleus is on the left, HST-1 is the variable feature to the right as noted on the top image of each column. The observation date is on the upper left hand corner of each image. The total jet length shown in these images is about 3″ or 230 parsecs. The jet has been rotated to be aligned with the horizontal axis.
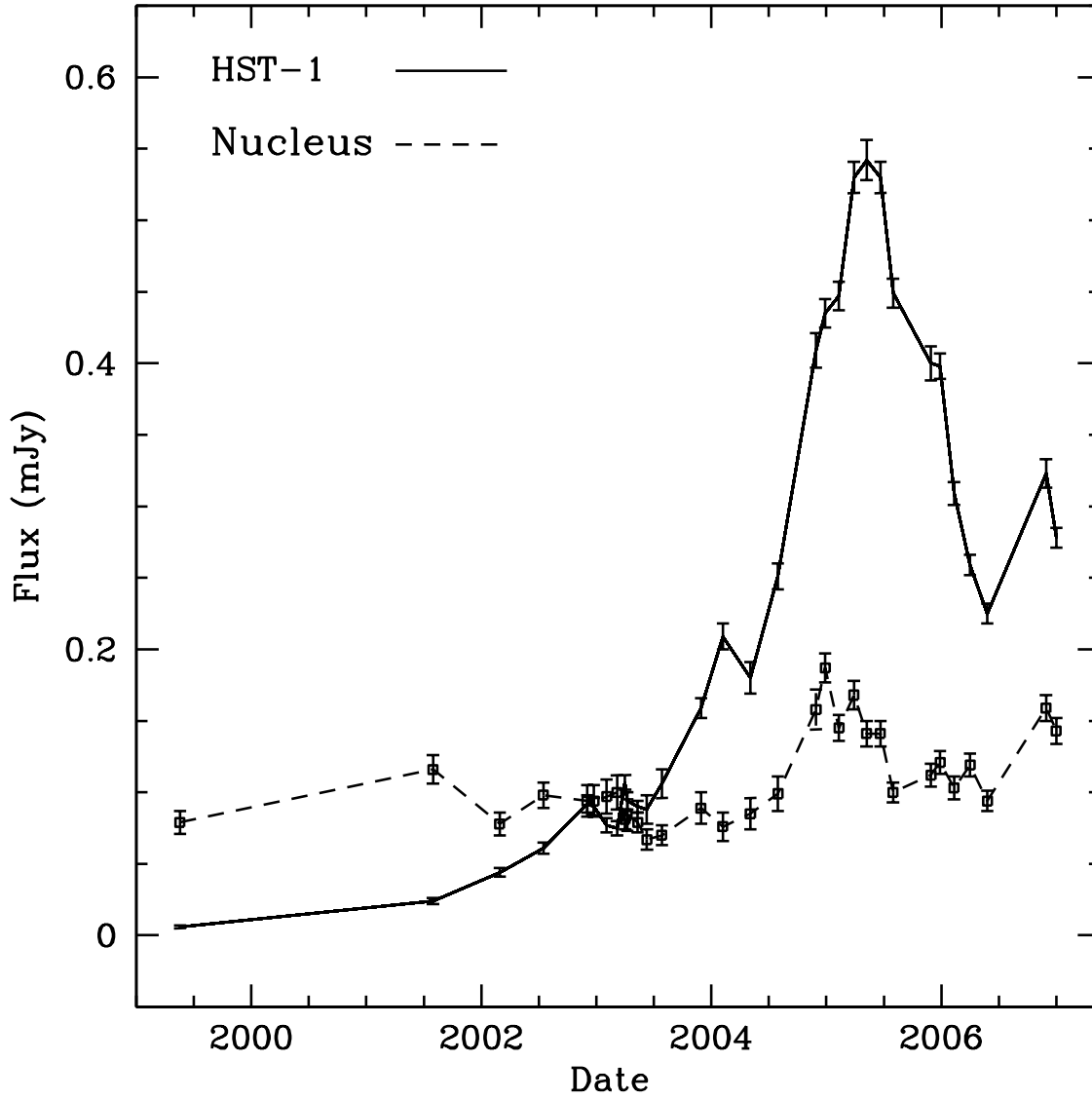
Fig. 2.— NUV light curve for knot HST-1 and the nucleus of M87 from May 1999 to December 2006, in units of milliJanskys (mJy), $1Jy = 10^{-26}WHz^{-1}m^{-2}$.
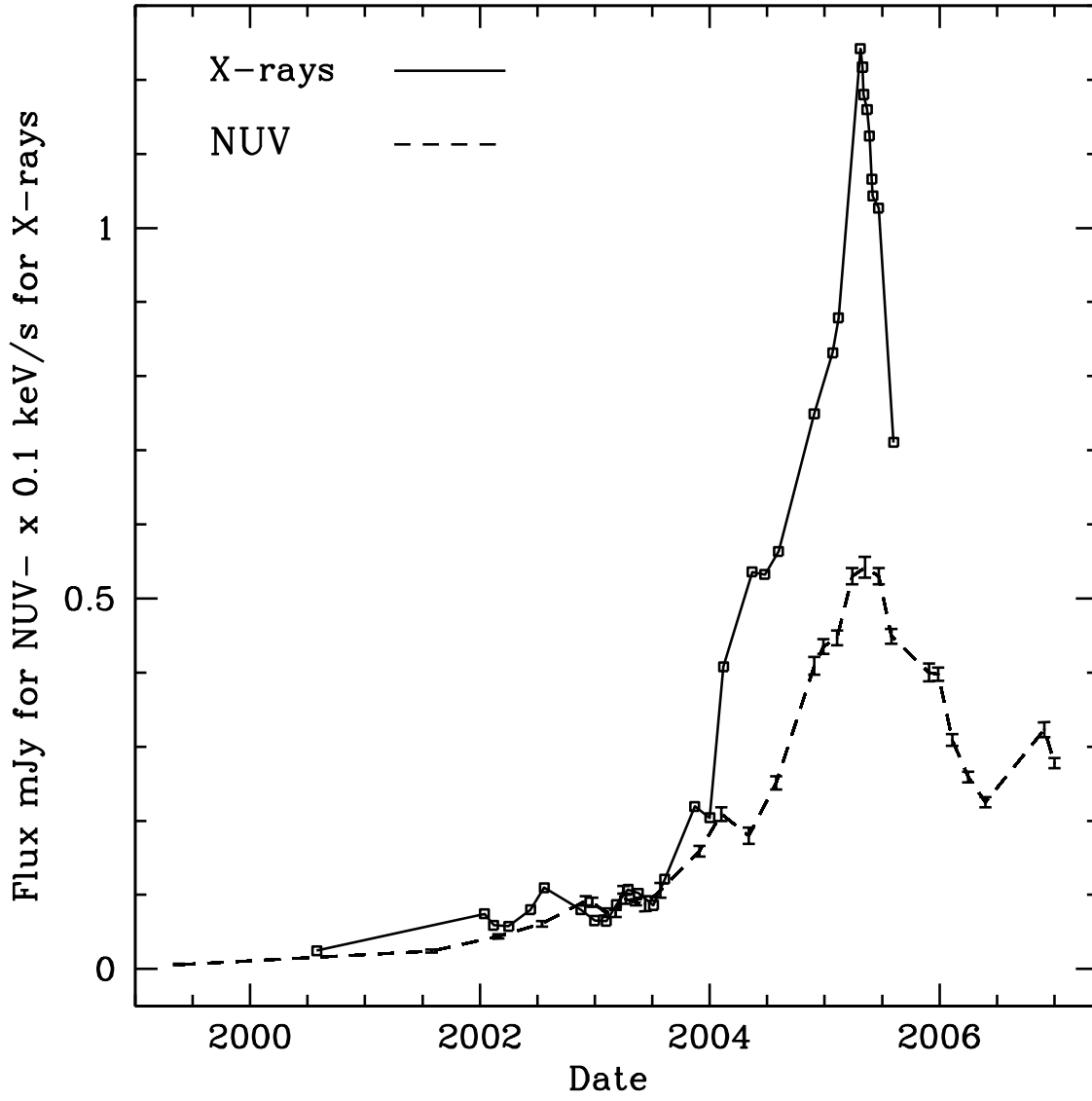
Fig. 3.— NUV and X-ray light curves of HST-1. The X-ray data was taken from Harris et al. (2006).

Table 1.   Log of observations and NUV intensities of the Nucleus and HST-1

Date	Camera/Filter	Nucleus	HST-1
1999 May 17	STIS/F25QTZ	0.079 ± 0.008	0.006 ± 0.001
2001 Jul 30	STIS/F25QTZ	0.116 ± 0.010	0.024 ± 0.002
2002 Feb 27	STIS/F25QTZ	0.078 ± 0.008	0.044 ± 0.003
2002 Jul 17	STIS/F25QTZ	0.098 ± 0.009	0.061 ± 0.004
2002 Nov 30	ACS/F220W	0.094 ± 0.011	0.092 ± 0.006
2002 Dec 22	ACS/F220W	0.094 ± 0.011	0.090 ± 0.006
2003 Feb 02	ACS/F220W	0.097 ± 0.012	0.077 ± 0.005
2003 Mar 06	ACS/F220W	0.100 ± 0.012	0.075 ± 0.005
2003 Mar 31	ACS/F250W	0.081 ± 0.007	0.107 ± 0.005
2003 Apr 07	ACS/F220W	0.084 ± 0.011	0.094 ± 0.006
2003 May 10	ACS/F250W	0.079 ± 0.007	0.090 ± 0.004
2003 Jun 7	STIS/F25QTZ	0.067 ± 0.007	0.088 ± 0.010
2003 Jul 27	STIS/F25QTZ	0.070 ± 0.007	0.106 ± 0.010
2003 Nov 29	ACS/F220W	0.089 ± 0.011	0.159 ± 0.007
2004 Feb 07	ACS/F220W	0.076 ± 0.010	0.209 ± 0.009
2004 May 05	ACS/F220W	0.085 ± 0.011	0.180 ± 0.011
2004 Jul 30	ACS/F220W	0.099 ± 0.012	0.251 ± 0.009
2004 Nov 28	ACS/F220W/F250W	0.158 ± 0.014	0.409 ± 0.012
2004 Dec 26	ACS/F250W	0.187 ± 0.010	0.435 ± 0.010
2005 Feb 09	ACS/F250W	0.145 ± 0.009	0.447 ± 0.010
2005 Mar 27	ACS/F250W	0.168 ± 0.010	0.530 ± 0.011
2005 May 09	ACS/F220W/F250W	0.141 ± 0.009	0.542 ± 0.014
2005 Jun 22	ACS/F250W	0.141 ± 0.009	0.530 ± 0.011
2005 Aug 01	ACS/F250W	0.100 ± 0.007	0.449 ± 0.010
2005 Nov 29	ACS/F220W/F250W	0.112 ± 0.008	0.400 ± 0.012
2005 Dec 26	ACS/F250W	0.121 ± 0.008	0.398 ± 0.009
2006 Feb 08	ACS/F220W/F250W	0.103 ± 0.008	0.309 ± 0.008
2006 Mar 30	ACS/F250W	0.119 ± 0.008	0.259 ± 0.007
2006 May 23	ACS/F220W/F250W	0.094 ± 0.007	0.225 ± 0.007
2006 Nov 28	ACS/F220W/F250W	0.159 ± 0.009	0.323 ± 0.010
2006 Dec 30	ACS/F250W	0.143 ± 0.009	0.278 ± 0.007

Note. — Col. (1), observation dates; col. (2), camera and filter in use; col (3), nucleus flux and poisson error in milliJanskys; col. (4), flux and poisson error for HST-1 in milliJanskys.

Table 2.   NUV doubling and halving times (DT and HT) for HST-1

Epoch Interval	Δt	y-1	DT	HT
1999 May 17 - 2001 Jul 30	2.21	3.00	0.73	
2001 Jul 30 - 2002 Feb 27	0.58	0.83	0.70	
2002 Feb 27 - 2002 Jul 17	0.38	0.39	0.97	
2002 Jul 17 - 2002 Nov 30	0.37	0.51	0.72	
2002 Nov 30 - 2002 Dec 22	0.06	0.02		1.50
2002 Dec 22 - 2003 Feb 02	0.12	0.14		0.43
2003 Feb 02 - 2003 Mar 06	0.09	0.03		1.50
2003 Mar 06 - 2003 Mar 31	0.07	0.43	0.16	
2003 Mar 31 - 2003 Apr 07	0.02	0.12		0.08
2003 Apr 07 - 2003 May 10	0.09	0.04		1.13
2003 May 10 - 2003 Jun 07	0.08	0.22		0.18
2003 Jun 07 - 2003 Jul 27	0.14	0.21	0.67	
2003 Jul 27 - 2003 Nov 29	0.34	0.50	0.68	
2003 Nov 29 - 2004 Feb 07	0.19	0.31	0.61	
2004 Feb 07 - 2004 May 05	0.24	0.14		0.85
2004 May 05 - 2004 Jul 30	0.24	0.39	0.61	
2004 Jul 30 - 2004 Nov 28	0.33	0.63	0.52	
2004 Nov 28 - 2004 Dec 26	0.08	0.06	1.33	
2004 Dec 26 - 2005 Feb 09	0.12	0.03	4.44	
2005 Feb 09 - 2005 Mar 27	0.12	0.19	0.63	
2005 Mar 27 - 2005 May 09	0.12	0.02	5.22	
2005 May 09 - 2005 Jun 22	0.12	0.02		5.22
2005 Jun 22 - 2005 Aug 01	0.11	0.15		0.36
2005 Aug 01 - 2005 Nov 29	0.33	0.11		1.50
2005 Nov 29 - 2005 Dec 26	0.07	0.01		3.50
2005 Dec 26 - 2006 Feb 08	0.12	0.22		0.27
2006 Feb 08 - 2006 Mar 30	0.14	0.16		0.44
2006 Mar 30 - 2006 May 23	0.15	0.13		0.57
2006 May 23 - 2006 Nov 28	0.52	0.44	1.18	
2006 Nov 28 - 2006 Dec 30	0.09	0.14		0.32

Note. — Col. (1), dates; col. (2), Δt time interval in years ; col (3), y-1 where y=I_2/I_1, 1-y if $I_2 < I_1$; col. (4), doubling time (DT) or halving time (HT).

REFERENCES

Aharonian, F. et al. 2006, Science, 314, 1424

Bicknell, G. V. & Begelman, M. C. 1996, ApJ, 467, 597

Bohlin, R. C. 2007, Photometric Calibration of the ACS CCD cameras, ACS Instrument Science Report 2007-06, (Baltimore: STScI)

Cardelli, J. A., Clayton, G. C., & Mathis, J. S. 1989, ApJ, 345, 245

Cheung, C., Harris, D. E., & Stawarz, L. 2007, ApJL, 663, L65

Gonzaga, S. et al. 2005, ACS Instrument Handbook, Version 6.0, (Baltimore: STScI)

Hardcastle, M. J. et al. 2007, ApJL, 670, L81

Harris, D. E., & Krawczynski, H. 2002, ApJ, 565, 244

Harris, D. E. 2003, New Astronomy Reviews, 47, 617

Harris, D. E., Biretta, J. A., Junor, W., Perlman, E. S., W. B., Sparks, W., Wilson, A. S. 2003, ApJ, 586, L41

Harris, D. E., Cheung, C. C., Biretta, J. A., Sparks, W. B., Junor, W., Perlman, E. S., Wilson, A. S. 2006, ApJ, 640, 211

Harris, D. E., & Krawczynski, H. 2006, ARA&A, 44, 463

Harris, D. E., Cheung, C. C., Stawarz, L., & Perlman, E. S. 2008 submitted

Kim Quijano, J., et al. 2003, STIS Instrument Handbook, version 7.0, Baltimore, STScI

Koekemoer, A. M., Fruchter, A. S., Hook, R. N., & Hack,W. 2002, in The 2002 HST Calibration Workshop: Hubble after the Installation of the ACS and the NICMOS Cooling System, ed. S. Arribas, A. Koekemoer, & B. Whitmore, Baltimore, STScI, 339

Laidler, V., et al. 200, Synphot User's Guide, version 5.0, Baltimore, STScI

Lauer, T. R. et al. 1992, AJ, 103, 703

Mack, J., et al. 2003, ACS Data Handbook, Version 2.0 (Baltimore: STScI),

Madrid, J. P., Sparks, W. B., Harris, D. E., Perlman, E. S., Macchetto, D., Biretta, J. 2007, Ap&SS, 311, 329

Perlman, E. S., Biretta, J. A., Sparks, W. B., Macchetto, F. D., & Leahy, J. P. 2001, ApJ, 551, 206

Perlman, E. S., Harris, D. E., Biretta, J. A., Sparks, W. B., & Macchetto, F. D. 2003, ApJ, 599, L65

Proffitt, C. R., Brown., T. M., Mobasher, B., & Davies, J. 2003 Instrument Science Report, STIS 2003-01, (Baltimore: STScI)

Schlegel, D. J, Finkbeiner, D. P., & Davis, M. 1998, ApJ, 500, 525

Sirianni, M., et al. 2005, PASP, 117, 1049

Stawarz, L. et al. 2006, MNRAS, 370, 981

Ulrich, M. E., Marashi, L., Urry, C. M., 1997, ARA&A, 35, 445

Tonry, J. L. et al. 2001, ApJ, 546, 681

Wall, J. V. & Jenkins, C. R. 2003, Practical Statistics for Astronomers, Cambridge University Press

Waters, C. Z., & Zepf, S. E. 2005, ApJ, 624, 656